Influence of temperature cycling and pore fluid on tensile strength of chalk

Voake, T.; Nermoen, A.; Ravnås, C.; Korsnes, R. I.; Fabricius, I.L.

Published in:
Journal of Rock Mechanics and Geotechnical Engineering

Link to article, DOI:
10.1016/j.jrmge.2018.12.004

Publication date:
2019

Document Version
Publisher's PDF, also known as Version of record

Journal of Rock Mechanics and Geotechnical Engineering 11 (2019) 277–288

Contents lists available at ScienceDirect

Journal of Rock Mechanics and Geotechnical Engineering

journal homepage: www.rockgeotech.org

Full Length Article

Influence of temperature cycling and pore fluid on tensile strength of chalk

T. Voake [a,b,*], A. Nermoen [b,c], C. Ravnås [d], R.I. Korsnes [a,b], I.L. Fabricius [a,d]

[a] University of Stavanger, Stavanger, Norway
[b] The National IOR Center of Norway, University of Stavanger, Stavanger, Norway
[c] NORCE Norwegian Research Centre AS, Oslo, Norway
[d] Technical University of Denmark, Copenhagen, Denmark

ARTICLE INFO

Article history:
Received 23 April 2018
Received in revised form
10 December 2018
Accepted 28 December 2018
Available online 28 January 2019

Keywords:
Tensile strength
Weakening by heating and cooling cycles
Anisotropic thermal expansion

ABSTRACT

Calcite has a highly anisotropic thermal expansion coefficient, and repeated heating and cooling cycles can potentially destabilize chalks by breaking cement bonds between neighboring particles. Based on tensile strength measurements, we investigated how temperature cycles induce weakening of chalk. Tensile strength tests were performed on chalk specimens sampled from Kansas (USA) and Mons (Belgium), each with differing amounts of contact cement. Samples of the two chalk types were tested in dry and water-saturated states, and then exposed to 0, 15, and 30 temperature cycles in order to find out under what circumstances thermally induced tensile strength reduction occurs. The testing results show that the dry samples were not influenced by temperature cycling in either of the chalk types. However, in the water-saturated state, tensile strength is increasingly reduced with progressive numbers of temperature cycles for both chalk samples, especially for the more cemented Kansas chalk. The Kansas chalk demonstrated higher initial tensile strength compared to the less cemented Mons chalk, but the strength of both chalks was reduced by the same relative proportion when undergoing thermal cycles in the water-saturated state.

1. Introduction

Carbonates are important reservoir rocks, which account for 50%–60% of the world's petroleum reserves (Burchette, 2012). Mechanical integrity of chalk has triggered a significant interest in engineering and academic circles since it was noticed that the sea bed over the Ekofisk oil field on the Norwegian Continental shelf subsided due to reservoir depletion (Sulak and Danielsen, 1988). Besides the reduction of pore pressure and then the increase in effective stress, compaction was later found to be enhanced by flooding with water (Hermansen et al., 1997). This so-called water weakening has been widely studied, but the potential effect of repeated temperature cycling of an initially warm reservoir cooling down due to the injection of cold water and then re-warming to equilibrate when this injection stops during the production life of an oil field has attracted less attention.

Chalk is a sedimentary rock with the main component of diagenetically altered calcareous nannofossils, which have calcite as a main component. Marble is a metamorphosed rock also composed of calcite, and experiments have shown that its strength is significantly influenced by temperature fluctuations. For example, marble monuments experience degradation and some marble façades tend to experience concave bowing when exposed to outdoor temperature variation (Weiss et al., 2003). Hansen et al. (2003) explored this phenomenon by comparing flexural strengths of naturally exposed marble to that of laboratory tested marble at 0% and 100% relative humidity. They found that naturally exposed marble weakens with respect to the number of years exposed, and the marble tested at 100% relative humidity weakens with the number of cooling and heating cycles, whereas no such trend was observed on dry samples tested.

Freshly deposited calcareous ooze has porosity of approximately 70%, and as it gets buried in depth, the ooze is mechanically compacted by overburden stress, resulting in pore volume loss. As the ooze is buried deeper, the stress at particle contacts builds up, resulting in pressure dissolution and contact cement, forming chalk (Fabricius, 2014). However, the strength development of chalk is

* Corresponding author.
E-mail address: tijana.voake@uis.no (T. Voake).
Peer review under responsibility of Institute of Rock and Soil Mechanics, Chinese Academy of Sciences.

https://doi.org/10.1016/j.jrmge.2018.12.004

not fully understood, and two strength components are suggested: attractive van der Waals forces at the contact cement and repulsive electrostatic forces between particles separated by water (Nermoen et al., 2018). Calcite is a uniaxial crystal with large anisotropic thermal expansion coefficients, which could induce stresses at cemented particle contacts when temperatures vary (Table 1). Two scenarios are considered here where the crystallographic *c*-axis of two neighboring particles parallel and perpendicular to each other (Fig. 1). Crystallographic axis perpendicular to *c*-axis is referred to as *a*-axis. Upon heating, in scenario 1, the particles contract in the plane perpendicular to the *c*-axis, resulting in the two particles being pulled apart and creating tensile forces at their contact cement (Fig. 1a); in scenario 2, the contact cement experiences shear forces as the contact area on one particle is contracting and the area on the other particle is expanding (Fig. 1b). These are two end member scenarios that most contact in a porous rock would fall in between. Once the contact cement bond is broken, it cannot be readily re-established; hence the premise of this paper is to investigate to what extent temperature variation induces loss in tensile strength of two chalk types.

Subcritical fracturing is considered as the main mechanism for stress corrosion, and propagation of pre-existing fractures during rock failure (Atkinson, 1984). The fracture depends on rock fabric, surrounding environments, and levels of applied stress. During subcritical fracturing of quartz, the fracture velocity was found to be much higher when water instead of air is present nearby the fracture tip. Additionally, the chemical species dissolved in the water, making it more polar, also play a role (Atkinson and Meredith, 1981). For limestone in which the primary mineral constituent is calcite, Lisabeth and Zhu (2015) demonstrated that the samples tested with equilibrated water were stronger than those tested with distilled water, and microcracking was the dominant deformation mechanism at lower pressures, while chemical weakening and twinning were more important for elevated pressures.

To understand how the pore fluid alters sample strength, a closer look at the surface properties of the mineral and its interaction with the ions dissolved in the water phase is required. The calcite surface has charged sites (Stipp, 1999). The cleavage plane $\{10\bar{1}4\}$ is populated with partially charged Ca^{2+} and CO_3^{2-}, thus, when a polar fluid is introduced to pore space, such as water, it is absorbed on the calcite surface, and a repulsive double-layer is created, making the chalk weaker (Megawati et al., 2013; Nermoen et al., 2018). The thickness of the double-layer, as described by the Debye–Hückel theory, increases with temperature (Andreassen and Fabricius, 2010), and is characterized by the Debye length κ^{-1} (Lyklema, 2000):

$$\kappa^{-1} = \left(\frac{\varepsilon_0 \varepsilon_r k_b T}{2 N_A e^2 I}\right)^{1/2} = \left[\frac{(8.85\times10^{-12})\varepsilon_r (1.38\times10^{-23})T}{2\times(6.02\times10^{23})\times(1.6\times10^{-19})^2 I}\right]^{1/2} \quad (1)$$

where ε_0 is the permittivity of a vacuum, ε_r is the relative permittivity of water (the saturating fluid), k_b is the Boltzmann's constant, T is the temperature, N_A is the Avogadro's number, e is the elementary charge, and I is the ionic strength of the pore water. The relative permittivity of water also depends on the temperature, which must be taken into account. ε_r is 88.44 at 20 °C and 51.17 at 130 °C (Yakaboylu et al., 2013). Repulsion increases with the thickness of the double-layer, because the volume in which the double layers overlap between two neighboring particles increases.

The surface energy γ_s of the cleavage plane $\{10\bar{1}4\}$ depends on the presence of water, and the surface energies of dry and fully hydrated calcite surfaces are 0.32 J/m^2 and 0.15 J/m^2, respectively (Royne et al., 2011). Hence, the energy necessary to form a dry surface (fracture) is double the energy required for the formation of a wet surface. The energy $U_{Surface}$ required to create a surface between two calcite particles is a function of the cross-sectional area A of the contact cement between two particles:

$$U_{Surface} = \gamma_s A \quad (2)$$

This can be compared to the elastic energy $U_{tensile}$ of the contact cement caused by thermal expansion/contraction. In scenario 1 (Fig. 1a) where neighboring particles pull apart during heating, a tensile fracture occurs when the elastic energy overcomes the surface energy. In one-dimension (1D) condition, the tensile energy is calculated as

$$U_{tensile} = \frac{1}{2} E(\alpha \Delta T)^2 V_p \quad (3)$$

where E is the calcite Young's modulus, and V_p is the volume of a particle. Hooke's law for general anisotropic materials linearly relates stress to strain by elastic constant c:

$$\sigma_{ij} = c_{ijkl}\varepsilon_{kl} \quad (4)$$

Using an abbreviated Voigt notation, four elastic subscripts for the elastic constant are reduced to two, so that each pair of $ij(kl)$ is replaced by IJ (Mavko et al., 2009). In a transversely isotropic case, which corresponds to a calcite crystal, the Young's modulus along *c*-axis, E_{33}, becomes

$$E_{33} = c_{33} - \frac{2c_{13}^2}{c_{11}+c_{12}} = 57.8 \text{ GPa} \quad (5)$$

where c_{11} = 149.9 GPa, c_{33} = 85.2 GPa, c_{12} = 57.9 GPa, and c_{13} = 53.5 GPa (Chen et al., 2001). The Young's modulus along the *a*-axis, E_{11}, is expressed as

$$E_{11} = c_{11} - \frac{c_{13}^2(-c_{11}+c_{12}) + c_{12}(-c_{33}c_{12}+c_{13}^2)}{c_{33}c_{11}-c_{13}^2} = 110.9 \text{ GPa} \quad (6)$$

When heated in scenario 2, one particle expands along the contact cement and the other contracts, resulting in the creation of a shear stress τ (Fig. 1b). The strain energy U_{Shear} created by strain depends upon the shear stress τ, shear angle β, and contact volume V_c:

$$U_{Shear} = \frac{1}{2}\tau\beta V_c \quad (7)$$

$$\tau = G/\beta \quad (8)$$

where G is the shear modulus, which also depends on the crystal orientation. For calcite, G_{33} corresponds to the shear modulus parallel to *c*-axis with $\theta = 0°$, and G_{11} perpendicular to *c*-axis with $\theta = 90°$:

Table 1
Calcite anisotropic thermal expansion coefficient in the literature.

Reference	Thermal expansion coefficient, α (10^{-6} K^{-1})	
	Parallel to *c*-axis	Perpendicular to *c*-axis
Rosenholtz and Smith (1949)	23.8	−5.2
Markgraf and Reeder (1985)	32.3	−2.8
Wu et al. (1995)	28.798	−5.371
Rao et al. (1968)	25.1	−3.68

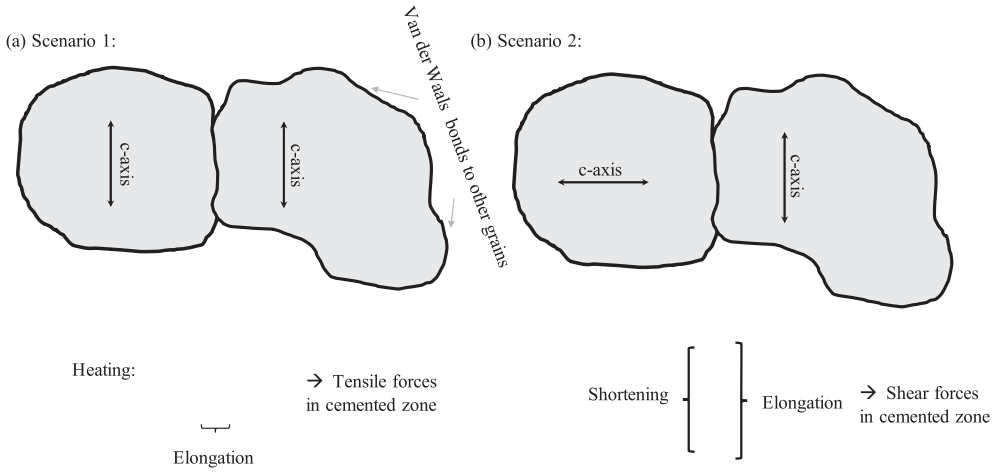

Fig. 1. Two scenarios in which the *c*-axis is (a) parallel and (b) perpendicular to each other dictate how the contact zone between neighboring calcite particles develop when the system is heated.

$$G = c_{66}\sin^2\theta + c_{44}\cos^2\theta \quad (9)$$

$$G_{33} = c_{66}\sin^2 0^\circ + c_{44}\cos^2 0^\circ = 34.1\ \text{GPa} \quad (10)$$

$$G_{11} = c_{66}\sin^2 90^\circ + c_{44}\cos^2 90^\circ = 45.8\ \text{GPa} \quad (11)$$

where c_{44} = 34.1 GPa (Chen et al., 2001), and $c_{66} = (c_{11}-c_{12})/2 = 45.8$ GPa.

As the tensile and shear energies depend on the particle volume, and the surface energy depends on the contact area between two particles, the elastic energy increases at a greater rate than the surface energy with increasing particle size. This would lead to larger particles breaking apart first, while smaller particles hold together.

Madland et al. (2002) experimentally studied how the tensile strength of highly porous chalk reduces when saturated with water or glycol at 130 °C compared with that tested at temperature 30 °C, while dry chalk showed no significant dependence of strength on temperature. Therefore, the temperature itself in the range of 30–130 °C is not likely to play a decisive role in determining the mechanical strength of chalks alone – for chalks it is the combination of pore fluid and temperature that together dictates sample strength within these temperature intervals. However, in the dry state, the dependence of strength on temperature has been observed in other materials including granite, gneiss, polymer mortars, as well as sandstone. They all demonstrated a strength reduction with increasing temperature (Jay, 1934; Lee et al., 1996; dos Reis, 2012; Huang and Xia, 2015).

Few studies have focused on how the material strength is affected by temperature cycles while performing strength tests at the same temperature. Hua et al. (2015) investigated how the tensile strength of sandstone samples depends on cyclical saturation with water for 48 h and drying at 105 °C for 24 h, and implied that 50% of strength was lost just after seven repeated cycles. Quartz, as the main component of sandstone, has an anisotropic thermal expansion coefficient of $14.4 \times 10^{-6}\ \text{K}^{-1}$ and $7.8 \times 10^{-6}\ \text{K}^{-1}$ in the direction perpendicular and parallel to the principal axis, respectively (Jay, 1934). Hence, the thermal anisotropy of quartz is not as pronounced as that of calcite.

In this paper, the effect of temperature cycling on chalks samples from two regions was studied by measuring tensile strength affected by 0, 15 and 30 temperature heating and cooling cycles. Furthermore, the tensile strengths of dry (air-saturated) and water-saturated samples are compared. The two chalks were selected due to their different degrees of induration and hence different degrees of contact cementation. Finally, the combined effects of pore fluid and temperature cycling on the two chalks are evaluated.

2. Materials and method

2.1. Materials

Chalks from two different quarries were used in this study: Kansas chalk from the Fort Hays Member of the Niobrara Formation (Late Cretaceous) located near Niobrara, Kansas, USA, and Mons chalk from the Trivières Formation (Late Cretaceous) located in Harmignies, Belgium. Kansas chalk has gone through a higher degree of diagenesis (Finn and Johnson, 2005) than the Mons chalk (Pirson et al., 2008). Ravnås (2017) found that the Mons chalk has a carbonate content of 99.8% and a Biot coefficient of 0.95; while the Kansas chalk has a carbonate content of 96.9% and a Biot coefficient of 0.91, which are lower than those of Mons chalk, indicating a higher degree of contact cement. Both chalks are homogeneous on the plug scale (Fig. 2).

Cylinders of about 40 mm in diameter and 300 mm in length were drilled perpendicular to the bedding from larger-size rock

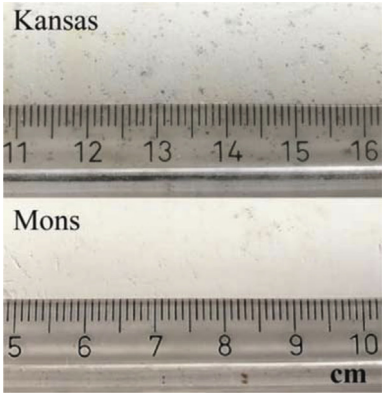

Fig. 2. Optical photography of Kansas and Mons chalks. The Kansas chalk has a higher content of microfossils seen as darker dots.

blocks (about 30 cm × 30 cm × 30 cm) from the two quarries. The long cylinders were then radially adjusted to 38.1 mm using a lathe, and cut into 156 disk-shaped samples with the length of 20–25 mm.

2.2. Petrographic and petrophysical characterizations

Characterization was performed on selected tested and untested samples. The untested samples were drilled from the same block as those for Brazilian test purposes.

For a visual assessment of the micro-structures of the chalk, polished samples were prepared, and backscatter electron micrographs were recorded using an FEI Inspect™ scanning electron microscope (SEM). The carbonate content was measured by dissolution of crushed samples using hydrochloric acid (HCl) and subsequent titration with NaOH. Based on the carbonate content measured by titration, a chalk sample large enough to yield 0.03 g of insoluble residue was dissolved in acetic acid. The non-carbonate minerals of the insoluble residue were identified by X-ray diffraction (XRD) using Cu K-α radiation and a PANalytical X'pert Pro X-ray Diffractometer.

P-wave velocity, v_p, of ultrasonic (200 kHz) elastic waves was recorded on dry cylindrical samples under uniaxial stress of 2 MPa (error: ±100 m/s). Based on the P-wave velocity and dry density ρ_d, the elastic P-wave modulus M was calculated as

$$M = \rho_d v_p^2 \tag{12}$$

The dry density ρ_d was measured using dry weight (error: ±0.01 g) and volume (error: ±0.044 cm^3) of a sample.

The grain density (ρ_g), nitrogen (N_2) porosity (ϕ), and permeability (k) were measured by using a PoroPerm Production 2 gas porosimeter from Vinci Technologies.

The specific surface area of crushed chalk samples (S_{BET}) was measured by a multipoint procedure using an Autosorb iQ gas sorption system from Quantachrome Instruments. This measured value was further used to derive the specific surface with respect to bulk volume (S_b) and that with respect to the porosity (S_ϕ):

$$S_b = S_{BET}\rho_g(1-\phi) \tag{13}$$

$$S_\phi = S_b/\phi \tag{14}$$

The equivalent cylindrical pore radius r then becomes

$$r = 2/S_\phi \tag{15}$$

By assuming an irreducible water film thickness h, the irreducible water saturation S_{wir} can be estimated by

$$S_{wir} = hS_\phi \tag{16}$$

The actual pore size distribution was measured by low-field nuclear magnetic resonance (NMR) spectrometry using a GeoSpec 2/53 DRX-HF digital spectrometer from Oxford Instruments. The recycle delay was set to 3750 ms, the number of echoes was 22,727, and echo spacing was 0.11 ms. Measurements were recorded at signal to noise ratio (SNR) greater than 500. Using Lithometrix, acquired data were converted into a relaxation time (T_2) distribution:

$$1/T_2 = \rho S_\phi \tag{17}$$

where ρ is a relaxation constant.

The NMR method sends polarizing pulses that excite hydrogen protons in the pore fluid, and then measures the signal decay rate of each pulse, which is also called the relaxation time. Pore walls cause rapid dephasing, so in smaller pores, an excited proton has a shorter distance to the pore wall, thus decaying in less time, and inversely the relaxation time is longer for larger pores.

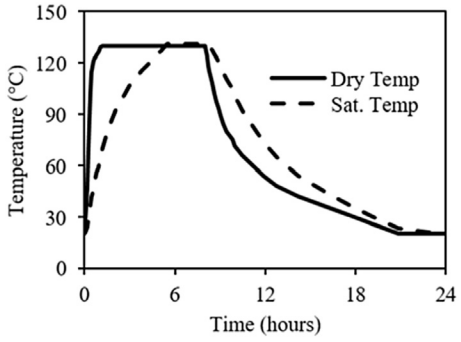

Fig. 3. A single temperature cycle for dry and saturated samples.

2.3. Brazilian tensile strength test

The disk-shaped samples from each location were randomly divided into two groups where half of the samples remained dry, and the others were saturated with calcite-equilibrated water of the ionic strength of 0.652 mmol/L (measured using ion chromatography). For each group, one third of samples were kept at room temperature (25 °C), while the remaining samples were repeatedly heated to 130 °C (8 h) and then cooled to room temperature (16 h). However, it took some time to reach the desired temperatures (Fig. 3). The target temperature was always reached within each cycle, and the samples were kept at the stable temperature for at least 1–2 h. During heating and cooling, the water-saturated samples were submerged in calcite-equilibrated water in a large steel container, which was kept at 3–5 bar (1 bar = 0.1 MPa) pressure to avoid evaporation and boiling.

The test matrix consists of chalks from two locations (Kansas and Mons), two saturation states (dry and water-saturated) and three kinds of cycles (0, 15 and 30). From each group, at 0, 15 and 30 temperature cycles, samples were randomly selected and their tensile strengths were measured by a Brazilian setup (Fig. 4). A total of 156 tensile tests were performed to obtain statistical confidence for the estimation of tensile strength.

Brazilian tests can measure the splitting tensile strength of brittle material. They were performed by subjecting each

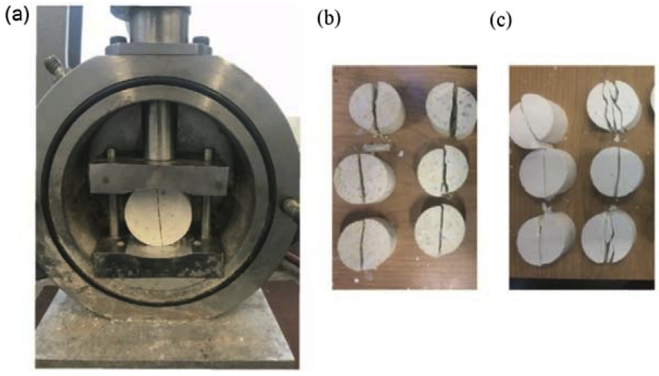

Fig. 4. (a) Brazilian test setup with a cylindrical chalk samples placed on the side between two parallelly loaded plates. Tensile fracture at failure is observed. (b) Optical photography of fractured Kansas chalk samples (15 cycles, dry). (c) Optical photography of fractured Mons chalk samples (15 cycles, dry).

cylindrical sample to load applied by two curved loading plates until the sample was split in half. Movement of the plates was controlled by injecting hydraulic oil with a Gilson 307 pump at a flow rate of 0.5 mL/min. Consequently, depending on the stiffness of the sample, the resulting loading rate will vary.

The normal force applied was measured by a transducer of type C2S and logged in a LabView routine. From the peak force (F) at which the sample fails, tensile strength (T_0) was calculated from the following equation:

$$T_0 = \frac{2F}{\pi Dt} \tag{18}$$

where D and t are the diameter and thickness of the disk, respectively.

3. Results

3.1. Petrographic and petrophysical characterizations

Using backscatter electron micrographs, we can observe the texture of the two chalk types (Figs. 5 and 6). The Kansas chalk has larger and more angular particles, as well as a larger contact area between the particles (Fig. 5). This is reflected in its higher induration of H3 (Henriksen et al., 1999). The Mons chalk has smaller particles and smaller contact areas between particles, as well as lower induration of H2 (Fig. 6). From Figs. 5 and 6, one can see that the frame of the rock is largely composed of calcite, whereas silicates and clays are rare, and do not contribute significantly to the frame. Hence, the analysis of the experimental results focuses on the temperature dependence on the contact between calcite particles.

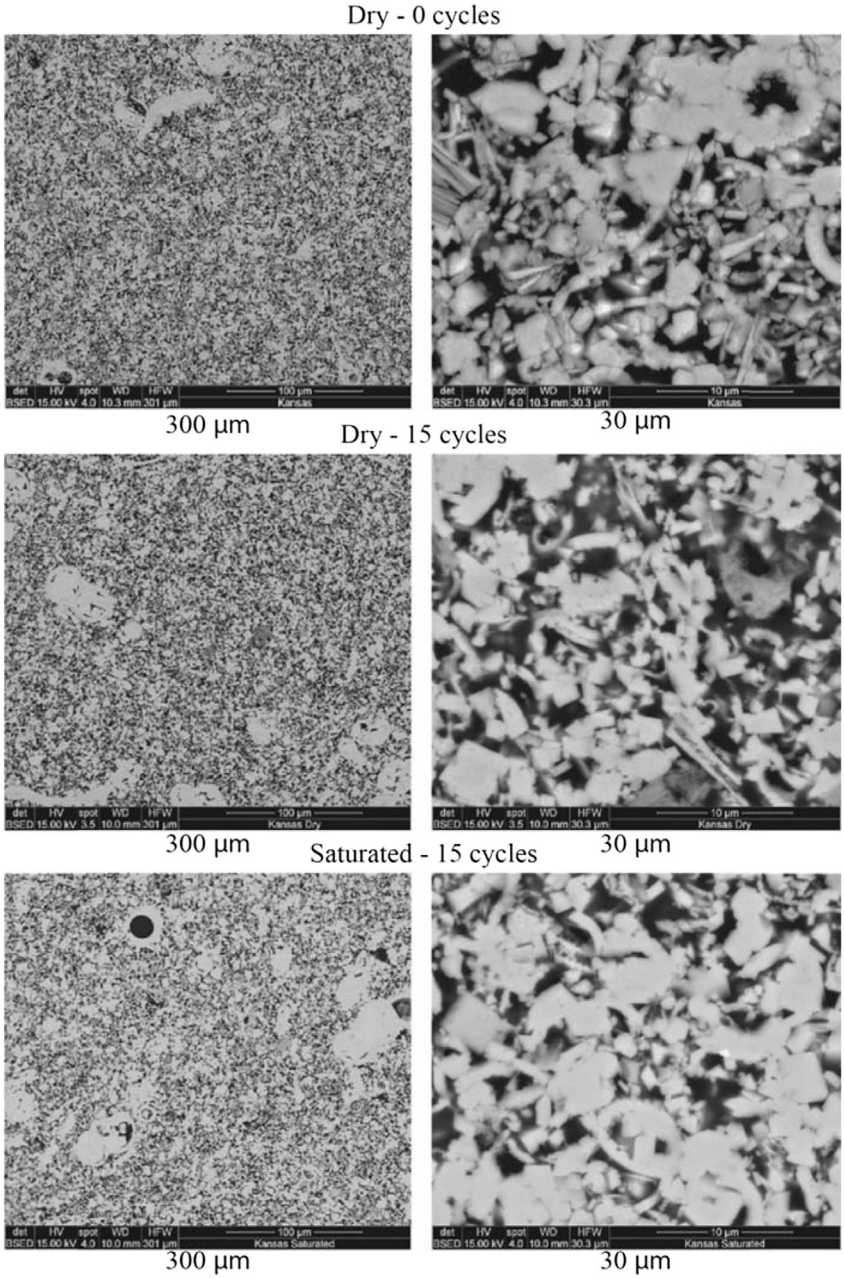

Fig. 5. Backscatter electron micrographs of Kansas chalk subjected to different numbers of temperature cycles in dry and saturated conditions.

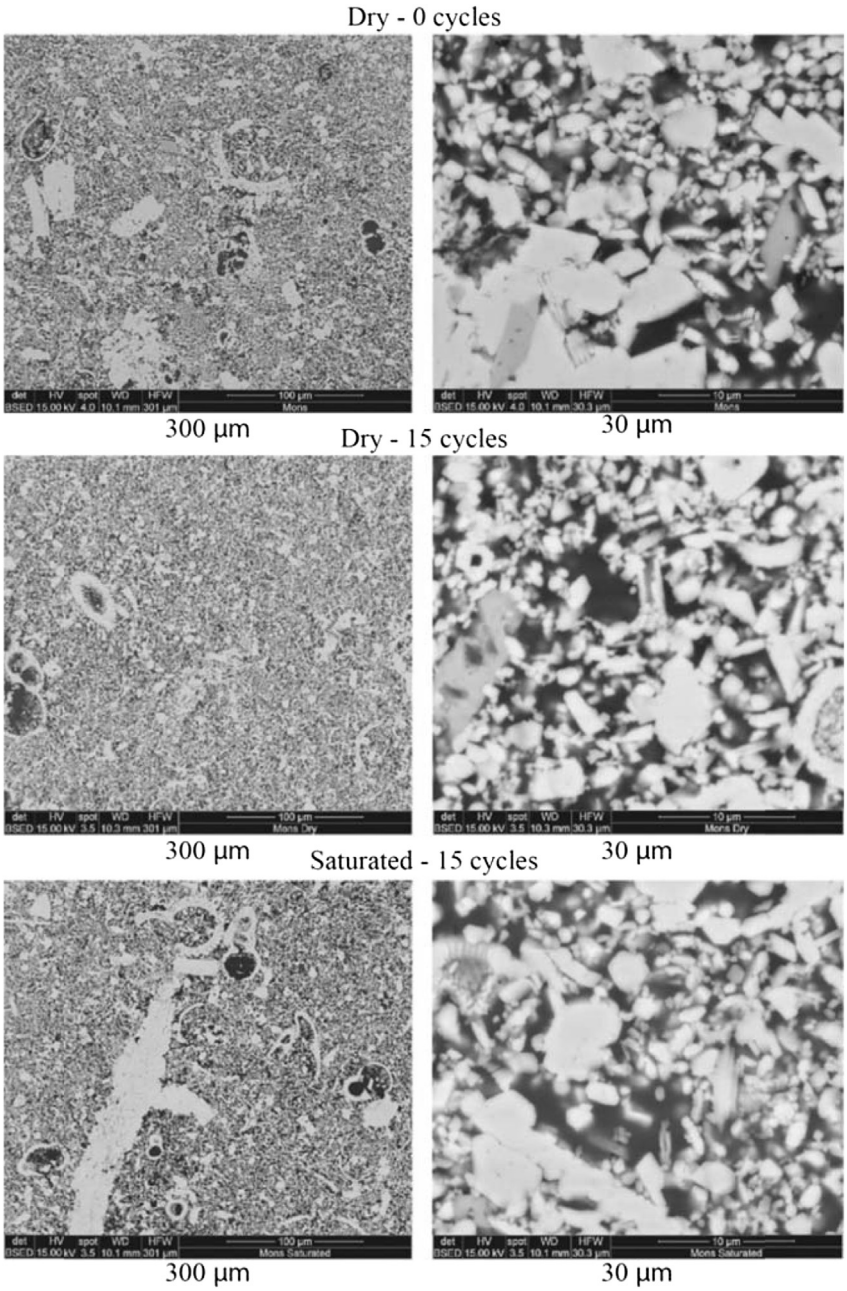

Fig. 6. Backscatter electron micrographs of Mons chalk subjected to different numbers of temperature cycles in dry and saturated conditions.

XRD analysis of the insoluble residue revealed that Kansas chalk also contains quartz, kaolinite and illite, as well as traces of feldspar, whereas Mons chalk contains smectite–illite and traces of apatite. It is evident that dry Kansas chalk has a higher P-wave modulus (M) than dry Mons chalk, indicating higher stiffness (Table 2).

Table 2
Carbonate content, mineral content and P-wave modulus (M) of dry Kansas and Mons chalk samples.

Chalk type	$CaCO_3$ content (%)	Error (%)	Other minerals	M (GPa)
Kansas	93.9–99.9	±0.1	Quartz, illite, kaolinite, and feldspar	14.4
Mons	99.6–99.9	±0.1	Smectite–illite, clinoptilolite, and apatite	9.5

In addition to the difference in mineralogy, Mons chalk has higher porosity and permeability than Kansas chalk. However, neither of these properties was significantly influenced by the temperature cycles (Table 3). Furthermore, as derived from S_{BET}, Mons chalk has a larger equivalent pore radius in comparison to Kansas chalk and therefore lower irreducible water saturation estimated. Only for Mons chalk did we find a significant increase in pore size due to temperature cycling (Table 3).

The increased pore size due to temperature cycling was further confirmed by the NMR data. Samples exposed to temperature cycling in the dry state indicated no change in the relaxation time (T_2) for Kansas chalk, whereas a shift to longer relaxation time was noticeable in all Mons chalk samples tested (Fig. 7). NMR measurements were performed on 4 samples from each location, all displaying the same trend, as shown in Fig. 7.

Table 3
Physical properties of Kansas and Mons chalks after 0 and 15 temperature cycles (dry samples).

Chalk type	Number of cycle	Porosity (%)	Permeability (mD)	S_{BET} (m^2/g)	Equivalent pore radius (nm)	Equivalent irreducible water saturation (%)
Kansas	0	34.2 ± 1.3	1.5 ± 0.3	2.8 ± 0.1	135 ± 7	7.3 ± 0.4
	15	34.5 ± 1.2	1.6 ± 0.3	2.6 ± 0.1	147 ± 6	6.7 ± 0.4
Mons	0	43.0 ± 1.0	2.7 ± 0.6	2.1 ± 0.1	260 ± 5	3.8 ± 0.3
	15	43.3 ± 0.9	2.7 ± 0.4	1.9 ± 0.1	299 ± 5	3.3 ± 0.3

Note: S_{BET} was measured for this study. The errors are estimated at a 95% confidence interval (Kaiser and Watters, 2012).

3.2. Brazilian tensile strength tests

A typical loading curve obtained in the LabView routine is shown in Fig. 8, in which the normal force acting on the two parallel planes is plotted as a function of time. The slope of the curve (red line) indicates the loading rate of that particular sample. The red dot indicates the maximum force that a sample could sustain before a fracture was formed (Fig. 4), leading to an abrupt drop in the measured normal force.

The tensile strengths of samples in each test series, which consisted of 10–15 samples for each given chalk type (Kansas and Mons), saturation state (dry and wet) and number of temperature cycles (0, 15 and 30 cycles), are shown in Table 4. In Fig. 9a and b, the tensile strength is arranged in ascending order, starting from the weakest samples on the left to the strongest ones on the right. Each line represents the results from the 10–15 samples in each series. Based on the distribution of strengths for each test series, the average value and standard deviation were determined and the Gaussian distribution was calculated (Fig. 9c and d). The tensile strengths of dry Kansas and Mons chalks showed no significant dependence on the number of temperature cycles. The increase in strength of dry Kansas chalk due to temperature cycling was considered insignificant when compared to the standard deviation. By contrast, the tensile strength of water-saturated samples for both chalks was reduced with an increasing number of temperature cycles (Fig. 9 and Table 4). Even though the standard deviation makes data overlap, there was a clear descending trend for the average values of saturated samples with increasing number of temperatures cycles, while this cannot be observed for the average values of dry samples. In addition, a distinct difference exists between 0 and 30 cycles for both chalks even when the standard deviation is taken into account for saturated samples; while again, there was no clear trend for dry samples. A positive correlation between the tensile strength and its standard deviation (σ) was observed, but all the standard deviations are found to be within 15%–30% of the average tensile strength T_0.

When comparing the impact of water saturation, before any temperature cycling was performed, the water weakening can be estimated for both chalk types. It was found that the initially stronger Kansas chalk was similarly susceptible to water weakening as Mons chalk (at zero cycle). The tensile strength of water-saturated Kansas and Mons chalks were 53% and 44% of the strength of dry samples, respectively. Since the Kansas chalk was initially stronger than Mons chalk, this implies that weakening by water saturation (in absolute terms) was 1.6 MPa for Kansas and 0.7 MPa for Mons chalk. The water-saturated Kansas chalk even had a lower tensile strength than the dry Mons chalk (Fig. 10a).

When increasing the number of temperature cycles in water-saturated conditions, the two chalks were weakened by the same absolute value (0.3 MPa) from 0 to 15 cycles (0.02 MPa/cycle). The strength reduction rate from 15 to 30 temperature cycles remained constant for Kansas chalk (0.3 MPa/15 cycles, or 0.02 MPa/cycle), but it was lower for Mons chalk (0.2 MPa/15 cycles, or 0.013 MPa/cycle). By the end of the 30th cycle, the proportion of strength reduction for saturated samples was almost equal for the two chalk types (Fig. 10b). However, if the temperature cycling effect is combined with the presence of pore fluid, comparing the dry and saturated samples subjected to 15/30 cycles, it is found that the Kansas chalk was more affected in terms of the absolute tensile strength loss (Fig. 11).

The significant change in tensile strength associated with water saturation was not caused by variations in porosity (Fig. 12), where no correlation was observed between the porosity and the tensile strength. However, due to the way in which the setup was designed and the flow rate of the hydraulic oil was controlled to supply the piston, the loading rate was affected by the stiffness of the sample,

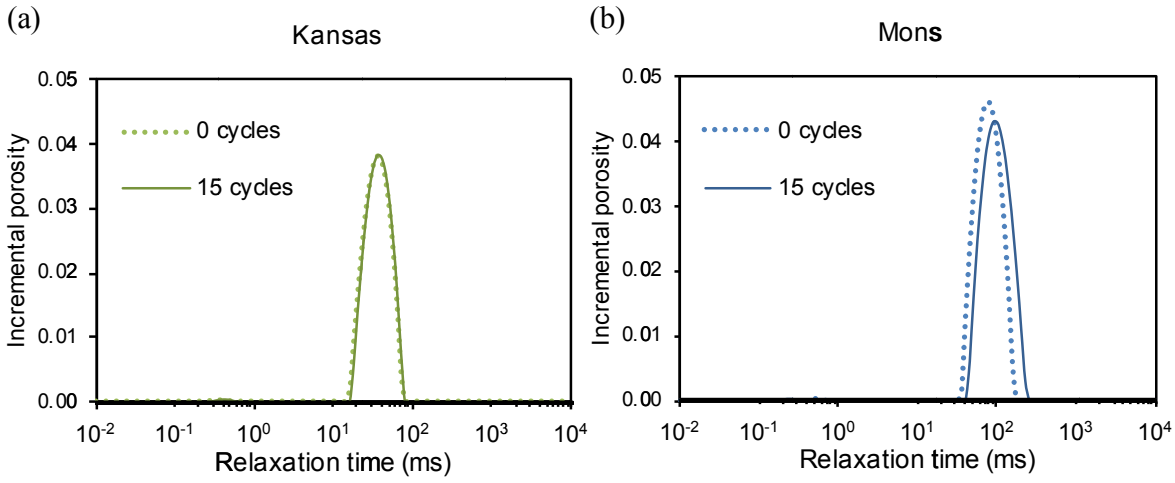

Fig. 7. Nuclear magnetic resonance (NMR) relaxation time after 0 and 15 temperature cycles in dry state. The NMR measurements were done after saturating these samples with water.

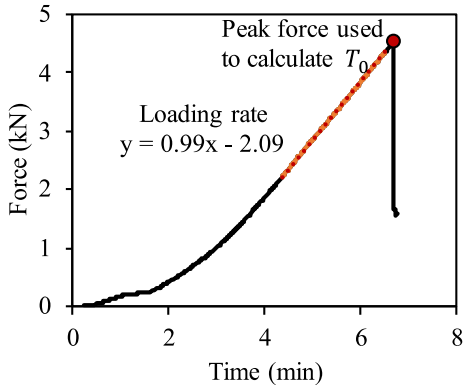

Fig. 8. Loading curve of a typical Brazilian test (dry Kansas sample). The curve was used to estimate the loading rate (red line) which correlates the stiffness of sample. The peak force is marked with the red dot and was used to estimate the tensile strength.

Table 4
Average values and standard deviations of the tensile strength measurements for each group of chalk samples. Even though the precision of the normal force measurement is high, the tensile strength for equally treated samples from the same block varies. As such, the tensile strength is presented only with one significant digit.

Chalk	State	Number of cycles	Number of samples	T_0 (MPa)	σ (MPa)	$T_{0dry}-T_{0sat}$ (MPa)
Kansas	Dry	0	10	3	0.4	–
		15	13	3.3	0.6	–
		30	10	3.3	0.6	–
	Saturated	0	14	1.4	0.2	1.6
		15	12	1.1	0.2	2.2
		30	12	0.8	0.2	2.5
Mons	Dry	0	13	1.6	0.3	–
		15	15	1.3	0.4	–
		30	15	1.4	0.4	–
	Saturated	0	13	0.9	0.2	0.7
		15	14	0.6	0.2	0.7
		30	15	0.4	0.1	1

and a strong correlation between the loading rate and tensile strength can be observed (Fig. 13). The stronger samples tend to have a higher loading rate, and the higher the loading rate, the stiffer the sample. From this relationship, it could be possible to predict the tensile strength from the loading rate without breaking the sample.

4. Discussion

In the dry state, we found no significant reduction in tensile strength with increasing number of temperature cycles for either Kansas or Mons chalk. Therefore, it seems that the contact cement is not influenced by the anisotropic thermal expansion of calcite particles in dry state. One significant change in the dry state was an increase in pore size of dry Mons chalk samples, although this difference was not observed for the dry Kansas chalk (Fig. 7). The change in pore size distribution agrees with the observed pore size increase calculated from S_{BET} data (Table 3), probably due to the clay alternation (smectite illitization) when heated at dry conditions. However, the process of dehydration of smectite does not seem to influence the tensile strength of the samples.

Our data show how water saturation immediately reduces the tensile strength of chalk before any temperature variation takes place (0 cycle). This is in line with other works (Madland et al., 2002; Risnes et al., 2005).

The 0.3 MPa reduction in tensile strength from 0 to 15 cycles implies that the saturated Mons chalk, by percentage, is more susceptible to weakening by the temperature cycling than Kansas chalk (33% and 21%, respectively), as it initially had lower tensile strength (Fig. 10b). Additionally, the tensile strength difference of the two samples was noticed when considering both the temperature cycling in combination with the saturation state, and a greater total difference in tensile strength was observed for the same number of temperature cycles, due to a constant dry tensile strength and a decrease in saturated tensile strength (Table 4).

It is observed that the water-saturated Kansas samples lost more initial tensile strength than Mons chalks, and even more so for 15 and 30 cycles (Fig. 11). Nevertheless, no significant difference was found in the relative behavior of Kansas and Mons chalks.

The tensile strength was constant for dry samples, but it decreased systematically for the water-saturated ones, suggesting that the contact cement bonds do not break in dry state but do in the water-saturated state. If we assume that weakening is caused by the breakage of bonds between neighboring particles, then the fact that the samples continued to weaken after the first 15 cycles implies that bond breakages are rare events compared to the number of bonds found in a sample. If this was not the case, all the bonds would break within the first initial temperature cycles and weakening of tensile strength would only be observed between 0 and 15 cycles, with no further reduction in tensile strength after 30 cycles. Since the Kansas samples had a constant weakening rate up to 30 cycles, whereas for Mons sample, the rate was reduced in 15–30 cycles, it could indicate that the overall number of bonds holding the sample together is less for Mons chalk than that for the Kansas chalk.

If it is assumed that the two scenarios shown in Fig. 1 hold, we can calculate the elastic strain energy of the bonds holding two neighboring chalk particles together, and then compare it to the energy needed to create a dry and water wet calcite surface between the particles as generated by breaking contact cement. By breaking the contact cement, two surfaces are created, one on each particle. If heating at 100 °C and a particle dimension of 10 μm are assumed, then the energies required to create either two dry or two wet surfaces are (using Eq. (2)):

$$U_{sur,dry} = 2 \times 0.32\,J/m^2 \times (10\,\mu m)^2 \times 10^{-12}\,m^2/(\mu m)^2 = 6.4 \times 10^{-11}\,J$$
$$U_{sur,sat} = 2 \times 0.15\,J/m^2 \times (10\,\mu m)^2 \times 10^{-12}\,m^2/(\mu m)^2 = 3 \times 10^{-11}\,J$$

It can be seen that the energy necessary to form a dry fracture is twice the energy required for the water-saturated fracture. Thus, the fracture growth in dry state is half of that in a saturated state.

In scenario 1 (Fig. 1), properties of contracting *a*-axis (perpendicular to *c*-axis) apply (E_{11}), and using Eq. (3), we can calculate the tensile elastic energy between two neighboring particles:

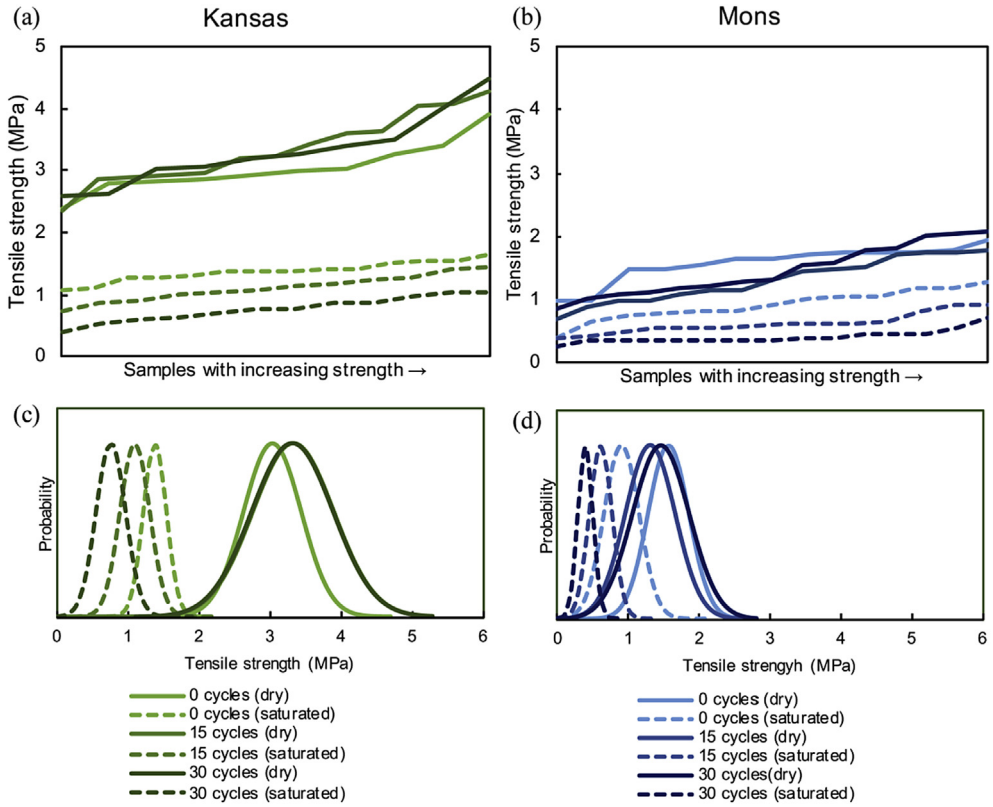

Fig. 9. Tensile strength from Brazilian tests on Kansas and Mons chalk samples in dry and saturated states subjected to varying number of temperature cycles. (a) and (b) represent individual samples for each group in increasing order from low (left) to high (right) tensile strength. (c) and (d) display the Gaussian distributions of each data set.

$$U_{\mathrm{el}} = 2 \times \frac{1}{2} \times 110.9 \times 10^{9}\ \mathrm{Pa} \times 5.2 \times 10^{-6} \times 100\ \mathrm{K} \times (10\ \mu\mathrm{m})^{2} \times 10^{-18}\ \mathrm{m}^{3} \Big/ (\mu\mathrm{m})^{3} = 2.3 \times 10^{-11}\ \mathrm{J}$$

This value is lower than the results of the energy required to create either two dry or two wet surfaces (6.4×10^{-11} J and 3×10^{-11} J, respectively), thus the tensile energy caused by the thermal contraction of *a*-axis between two particles is not enough to generate a fracture.

In scenario 2, where one side of a particle contracts and the other expands, the strain energy created by shearing is calculated by Eq. (7). If we again assume a particle of 10 μm in dimension, and that the shear zone thickness corresponds to a unit cell (*c*-axis = 17 Å) (Fig. 14), we can calculate the shear angle β from a ratio between the elongation and cemented area thickness:

$$\beta = \arctan\frac{\Delta x}{c\text{-axis}} = \arctan\frac{0.014\ \mu\mathrm{m}}{0.0017\ \mu\mathrm{m}} = 1.45^{\circ}$$

The relative displacement between particles is calculated by assuming a heating of 100 °C in which one side of the contact expands along *c*-axis while the other side contracts along the *a*-axis. We calculate the shear stress as the sum of shear stress along the top contacting contact (τ_{11}) and that along the bottom elongating contact (τ_{33}):

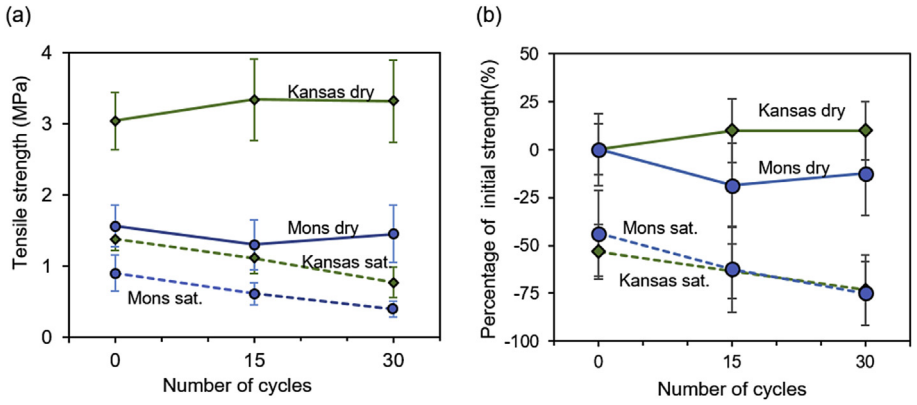

Fig. 10. (a) Average tensile strength and standard deviation as a function of number of temperature cycles. Dry and water-saturated samples are shown as solid and dashed lines, respectively. (b) Tensile strength difference (in %) as a function of temperature cycling, with the dry and 0 cycle for each chalk type as reference.

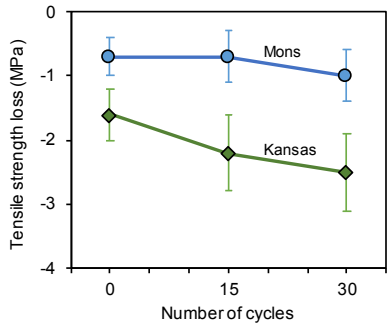

Fig. 11. Difference in tensile strength between dry and water-saturated samples for 0, 15 and 30 temperature cycles. The tensile strength of Kansas chalk was more reduced with an increasing number of temperature cycles than that of Mons chalk.

$$\tau_{11} = \frac{G_{11}}{\Delta x_{\text{top}}/c\text{-axis}} = \frac{45.8\ \text{GPa}}{2.94} = 15.6\ \text{GPa}$$

$$\tau_{33} = \frac{G_{33}}{\Delta x_{\text{bottom}}/c\text{-axis}} = \frac{34.1\ \text{GPa}}{13.53} = 2.5\ \text{GPa}$$

$$\tau = \tau_{11} + \tau_{33} = 18.1\ \text{GPa}$$

The elastic shear energy can thereby be calculated using Eq. (7):

$$U_{\text{shear}} = \frac{1}{2} \times 1.45 \times 1.81 \times 10^{10} \times (10 \times 10 \times 0.0017) \times 10^{-18}\ \text{m}^3 \big/ (\mu\text{m})^3 = 2.2 \times 10^{-9}\ \text{J}$$

As seen from the above results, the shear energy is greater than the energy needed to generate either dry or saturated calcite surfaces (6.4×10^{-11} J and 3×10^{-11} J, respectively). This is, however, an absolute upper limit. The two particles with orientations of *c*-axis perpendicular to each other are probably rare, and no weakening is found in dry samples. Scenarios 1 and 2 represent two extreme cases, and most neighboring particles are oriented with *c*-axis relative to each other in between those cases. The fact that we do not observe any weakening in dry samples indicates that the tensile and shear energies due to anisotropic thermal expansion are not sufficient to generate dry surfaces. However, the weakening by temperature cycling observed in water-saturated samples means that the energies are sufficient to generate water-saturated surfaces.

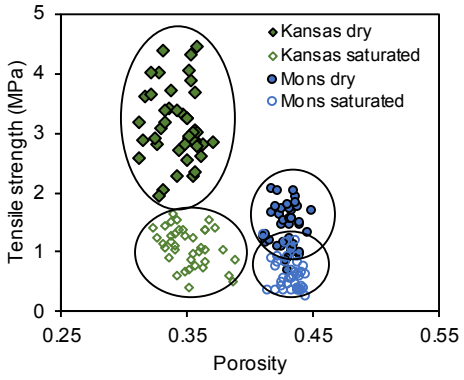

Fig. 12. Tensile strength plotted against the porosity of each sample. Mons chalk has a higher porosity than Kansas chalk and typically displays a lower strength. Water-saturated samples are weaker than dry samples. However, the porosity and the tensile strength do not correlate within individual chalk and saturated state.

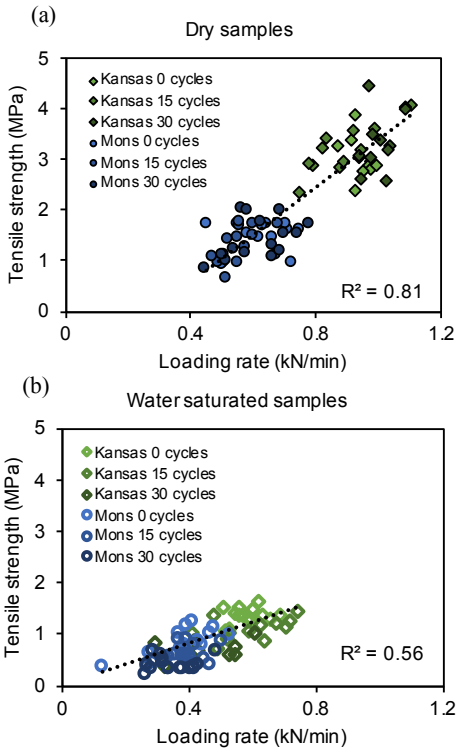

Fig. 13. Tensile strength plotted as a function of loading rate. Kansas chalk (green) is stronger than Mons chalk (blue). The strength of the dry samples (a) correlates better with loading rate than that of the saturated samples (b) with R^2 values of 0.81 and 0.56, respectively. No clear difference in strength is observed within the dry samples for an increasing number of temperature cycles (a), however, for the water-saturated samples, the loading rate is lowered by increasing the number of temperature cycles (b).

When the temperature is changed, fractures between particles may open gradually, and then water enters the fracture, inhibiting its closure when the temperature is reduced. This effect may be promoted by subcritical fracture processes which previously have shown to be driven by water. Even though the thermal cycling induces anisotropic thermal expansion of the calcite particles, irrespective of the pore fluid content, the tensile strength remains unchanged for the dry samples. However, for the water-saturated samples, the tensile strength is systematically reduced with increasing number of cycles for both chalks. This is in line with the behavior obtained in marble (Hansen et al., 2003). In our cases, the strength reduction induced by temperature cycling was more pronounced for the saturated Kansas chalk, which is more indurated than Mons chalk (Fig. 11). This indicates that water weakening phenomena play a role in the accumulated damage induced by the thermal cycles and can be linked to the understanding of how neighboring particles are held together. Royne et al. (2015) discussed how changes in nano-scale surface forces between two calcite particles developed using an atomic force microscope. They found that the forces between two calcite particles depend on the distance between the particles, which further depends on the water

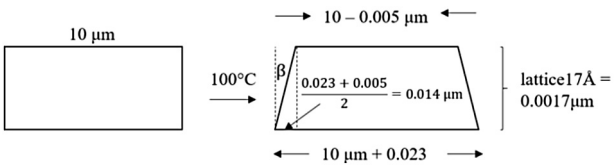

Fig. 14. Shear strain of contact between two 10 μm particles, caused by 100 °C heating.

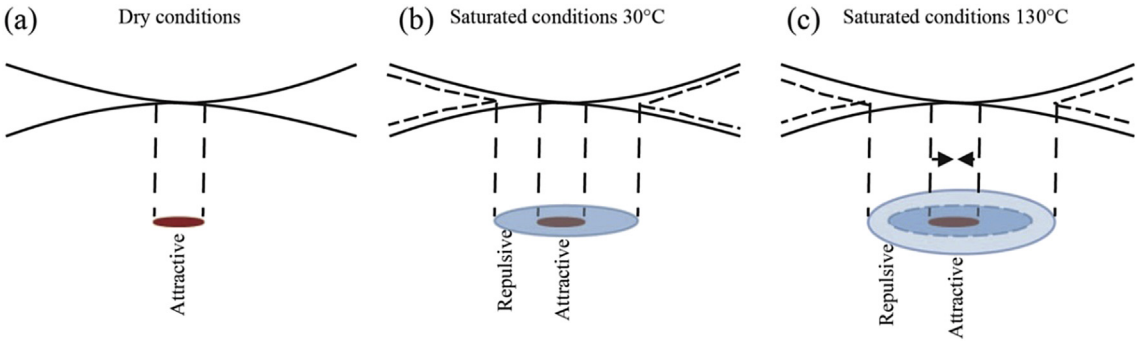

Fig. 15. Forces present between two calcite particles in (a) dry conditions, (b) water-saturated conditions at 30 °C, and (c) water-saturated conditions at 130 °C. An extra area of repulsive forces occurs at higher temperature associated with the increasing Debye length.

content. When there is no water present, only attractive forces pulling the particles together are observed. On the contrary, when water is present, a repulsive force is detected at intermediate practical distances, leading to a reduced cohesion between particles. The increased repulsion could facilitate the propagation of fractures that would not develop in the dry state, thereby creating greater repulsion and fracturing the contact cement. This thus weakens the samples as the number of temperature cycles is increased (Fig. 15). If we assume that the thickness of the charged layer is directly proportional to the Debye length, then the thickness of the layer depends on the temperature and increases with increasing temperature (Fig. 16). A thicker Debye length leads to an increase of repulsive area between the particles at higher temperatures, which causes further weakening of the water-saturated samples. As illustrated in Fig. 15c, not only the repulsive area increases, but also this increase may be sufficient to pull particles further apart, and water can then invade the fracture, reducing the attractive area.

To prevent dissolution/precipitation, we used calcite-equilibrated water as a saturating fluid. The equilibrated water was prepared at ambient temperature. Since the solubility is inversely correlated to temperature, the solution is over-saturated at higher temperatures. The solubility of calcite is 0.013 g/L, within one pore volume of each sample (approximately 10 mL). This amount reaches 0.00013 g of calcite that could precipitate, which would be less than 0.001% in weight compared to each sample (30 g). In addition, the solubility effect should only be observed by comparing the tensile strength in 0–15 cycles, and as such, increasing the number of cycles from 15 to 30 should not play a decisive role in tensile strength. This is because the maximum saturation has been achieved after the initial heating cycles. Therefore, it is conclusive that the effect observed in saturated samples is induced by temperature cycling, but not by dissolution/precipitation.

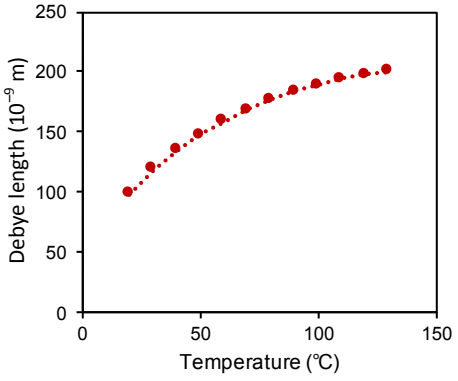

Fig. 16. Debye length increases with increasing temperature based on κ^{-1} equation (Eq. (1)).

5. Conclusions

Brazilian tests were performed to evaluate the influence of temperature cycling on the tensile strength of chalk in dry and water-saturated conditions. In dry conditions, neither Kansas chalk nor Mons chalk samples demonstrate weakening effects caused by temperature cycles. However, for both chalks, the initial tensile strength was halved by water saturation, and then further reduced with an increasing number of temperature cycles. For both chalks, the tensile strength of water-saturated samples after 30 temperature cycles was reduced to only 25% of the initial strength of dry samples that were not exposed to temperature cycling. The estimates showed that the energy needed to create new surfaces between neighboring particles held together by contact cement is higher than the thermoelastic energy induced by the heating of two adjacent particles with *c*-axes parallel to each other, but lower than the shear energy with *c*-axes perpendicular to each other. However, the probability of thermally induced cement bond fracture is higher in the water-saturated state because the surface energy is lower than that of dry calcite crystals. Presences of water and anisotropic thermal expansion of calcite are the driving weakening mechanisms when chalk is exposed to thermal cycling, while tensile strength experiments on dry samples detect no weakening by anisotropic thermal expansion alone.

Conflicts of interest

The authors wish to confirm that there are no known conflicts of interest associated with this publication and there has been no significant financial support for this work that could have influenced its outcome.

Acknowledgments

The authors acknowledge the Research Council of Norway and the industry partners, ConocoPhillips Skandinavia AS, Aker BP ASA, Eni Norge AS, Total E&P Norge AS, Equinor ASA, Neptune Energy Norge AS, Lundin Norway AS, Halliburton AS, Schlumberger Norge AS, Wintershall Norge AS, and DEA Norge AS, of the National IOR Center of Norway for support. We would also like to thank Espen Jettestuen (NORCE) for his contribution to numerically explaining forces between two neighboring calcite particles.

References

Andreassen KA, Fabricius IL. Biot critical frequency applied to description of failure and yield of highly porous chalk with different pore fluids. Geophysics 2010;75(6):E205–13.

Atkinson BK, Meredith PG. Stress corrosion cracking of quartz: a note on the influence of chemical environment. Tectonophysics 1981;77(1–2):T1–11.

Atkinson BK. Subcritical crack growth in geological materials. Journal of Geophysical Research: Solid Earth 1984;89(B6):4077–114.

Burchette TP. Carbonate rocks and petroleum reservoirs: a geological perspective from the industry. Geological Society, London, Special Publications 2012;370(1):17–37.

Chen CC, Lin CC, Liu LG, Sinogeikin SV, Bass JD. Elasticity of single-crystal calcite and rhodochrosite by Brillouin spectroscopy. American Mineralogist 2001;86(11–12):1525–9.

dos Reis JML. Effect of temperature on the mechanical properties of polymer mortars. Materials Research 2012;15(4):645–9.

Fabricius IL. Burial stress and elastic strain of carbonate rocks. Geophysical Prospecting 2014;62(6):1327–36.

Finn TM, Johnson RC. Niobrara total petroleum system in the Southwestern Wyoming Province. In: Petroleum systems and geologic assessment of oil and gas in the Southwestern Wyoming Province, Wyoming, Colorado, and Utah. US Geological Survey (USGS) Southwestern Wyoming Province Assessment Team; 2005.

Hansen KK, Leksø H, Grelk B. Assessment of the durability of marble cladding by laboratory exposure compared to natural exposure. In: Carmeliet J, Hens H, Vermeir G, editors. Research in building physics: proceedings of the 2nd international conference on building physics. CRC Press; 2003. p. 267–71.

Henriksen AD, Fabricius IL, Borre MK, Korsbech U, Theilgaard AT, Zandbergen JB. Core density scanning, degree of induration and dynamic elastic moduli of Palaeogene limestone in the Copenhagen area. Quarterly Journal of Engineering Geology 1999;32(2):107–17.

Hermansen H, Thomas LK, Sylte JE, Aasboe BT. Twenty five years of Ekofisk reservoir management. In: SPE annual technical conference and exhibition. Society of Petroleum Engineers (SPE); 1997. https://doi.org/10.2118/38927-MS.

Hua W, Dong SM, Li YF, Xu JG, Wang QY. The influence of cyclic wetting and drying on the fracture toughness of sandstone. International Journal of Rock Mechanics and Mining Sciences 2015;78:331–5.

Huang S, Xia KW. Effect of heat-treatment on the dynamic compressive strength of Longyou sandstone. Engineering Geology 2015;191:1–7.

Jay AH. The thermal expansion of bismuth by X-ray measurements. Proceedings of the Royal Society of London, Series A 1934;143(849):465–72.

Kaiser DL, Watters RL. Certificate of analysis. National Institute of Standards & Technology; 2012. https://www-s.nist.gov/srmors/certificates/1898.pdf.

Lee H, Lee H, Park Y, Kwon K. The mechanical and hydraulic characteristics of granite and gneiss under temperature variation. In: ISRM international symposium – EUROCK 96. Rotterdam: A.A. Balkema; 1996. p. 1371–7.

Lisabeth HP, Zhu WL. Effect of temperature and pore fluid on the strength of porous limestone. Journal of Geophysical Research: Solid Earth 2015;120(9):6191–208.

Lyklema J. Fundamentals of interface and colloid science. San Diego, USA: Academic Press; 2000.

Madland MV, Korsnes RI, Risnes R. Temperature effects in Brazilian, uniaxial and triaxial compressive tests with high porosity chalk. In: SPE annual technical conference and exhibition. SPE; 2002. https://doi.org/10.2118/77761-MS.

Markgraf SA, Reeder RJ. High-temperature structure refinements of calcite and magnesite. American Mineralogist 1985;70(5–6):590–600.

Mavko G, Mukerji T, Dvorkin J. The rock physics handbook: tools for seismic analysis of porous media. 2nd ed. Cambridge: Cambridge University Press; 2009.

Megawati M, Hiorth A, Madland MV. The impact of surface charge on the mechanical behavior of high-porosity chalk. Rock Mechanics and Rock Engineering 2013;46(5):1073–90.

Nermoen A, Korsnes RI, Storm EV, Stødle T, Madland MV, Fabricius IL. Incorporating electrostatic effects into the effective stress relation – insight from chalk experiments. Geophysics 2018;83(3):MR123–35.

Pirson S, Spagna P, Baele JM, Damblon F, Gerrienne P, Vanbrabant Y, Yans J. An overview of the geology of Belgium. In: Memoirs of the geological survey of Belgium. The 4th international meeting of anthracology, vol. 55. The Geological Survey of Belgium; 2008. p. 5–25.

Rao KVK, Naidu SVN, Murthy KS. Precision lattice parameters and thermal expansion of calcite. Journal of Physics and Chemistry of Solids 1968;29(2):245–8.

Ravnås C. Petrophysical and rock mechanical properties of heat treated chalk. Kongens Lyngby, Denmark: Technical University of Denmark; 2017.

Risnes R, Madland MV, Hole M, Kwabiah NK. Water weakening of chalk – mechanical effects of water-glycol mixtures. Journal of Petroleum Science and Engineering 2005;48(1–2):21–36.

Rosenholtz JL, Smith DZ. Linear thermal expansion of calcite, var. Iceland spar and Yule marble. American Mineralogist 1949;34:846–54.

Royne A, Bisschop J, Dysthe DK. Experimental investigation of surface energy and subcritical crack growth in calcite. Journal of Geophysical Research: Solid Earth 2011;116(B4):B04204.

Royne A, Dalby KN, Hassenkam T. Repulsive hydration forces between calcite surfaces and their effect on the brittle strength of calcite-bearing rocks. Geophysical Research Letters 2015;42(12):4786–94.

Stipp SLS. Toward a conceptual model of the calcite surface: hydration, hydrolysis, and surface potential. Geochimica et Cosmochimica Acta 1999;63(19):3121–31.

Sulak AM, Danielsen J. Reservoir aspects of Ekofisk subsidence. Journal of Petroleum Technology 1988;41(7):709–16.

Weiss T, Siegesmund S, Fuller ER. Thermal degradation of marble: indications from finite-element modelling. Building and Environment 2003;38(9–10):1251–60.

Wu TC, Shen AH, Weathers RS, Bassett WA, Chou IM. Anisotropic thermal-expansion of calcite at high-pressures – an in-situ x-ray-diffraction study in a hydrothermal diamond-anvil cell. American Mineralogist 1995;80(9–10):941–6.

Yakaboylu O, Harinck J, Smit KGG, de Jong W. Supercritical water gasification of manure: a thermodynamic equilibrium modeling approach. Biomass & Bioenergy 2013;59:253–63.

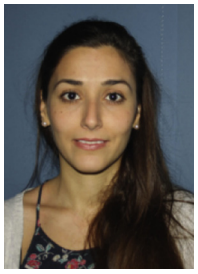

T. Voake is currently pursuing her PhD degree in Petroleum Technology at the University of Stavanger, Norway. She obtained her MSc degree in Geophysics from Memorial University of Newfoundland, and HBSc degree from the University of Toronto, Canada. She has worked on numerous field and laboratory projects classifying rock physical properties. She has previously worked in the petroleum industry for a software development company.